

## **A FAMILY OF ULTRA-THIN, POLARIZATION-INSENSITIVE, MULTI-BAND, HIGHLY ABSORBING METAMATERIAL STRUCTURES**

**Theofano M. Kollatou, Alexandros I. Dimitriadis\* ,  
Stylianos D. Assimonis, Nikolaos V. Kantartzis,  
and Christos S. Antonopoulos**

Department of Electrical and Computer Engineering, Aristotle University of Thessaloniki, Thessaloniki GR-54124, Greece

**Abstract**—The systematic design of size-confined, polarization-independent metamaterial absorbers that operate in the microwave regime is presented in this paper. The novel unit cell is additionally implemented to create efficient multi-band and broadband structures by exploiting the scalability property of metamaterials. Numerical simulations along with experimental results from fabricated prototypes verify the highly absorptive performance of the devices, so developed. Moreover, a detailed qualitative and quantitative analysis is provided in order to attain a more intuitive and sound physical interpretation of the underlying absorption mechanism. The assets of the proposed concept, applied to the design of different patterns, appear to be potentially instructive for various EMI/EMC configurations.

### **1. INTRODUCTION**

Metamaterials are artificial structures that exhibit unique electromagnetic properties not encountered in natural media, such as the negative refractive index and the magnetic activity of non-magnetic substances at optical frequencies. Actually, these remarkable features have inspired several applications in an assortment of engineering fields, like antennas, substrates, cloaking, and shielding [1, 2]. In their most frequent rendition, metamaterials comprise periodic arrays of metallic structures much smaller than the working wavelength and are typically described via effective medium theories, i.e., by extracting their effective constitutive parameters [3]. Recently, the scientific interest

---

*Received 31 December 2012, Accepted 19 January 2013, Scheduled 23 January 2013*

\* Corresponding author: Alexandros I. Dimitriadis (aldimitr@auth.gr).

has also focused on the application of metamaterials in the design of thin electromagnetic absorbers. In fact, the pioneering configuration proposed by Landy et al. [4] has attracted many researchers in the analysis and fabrication of absorbing devices that operate in the microwave, terahertz, and even visible frequencies [5–9]. Essentially, initial concepts have been realized on low-cost FR4 substrates by means of standard photolithographic techniques and proven to be very subwavelength, with a thickness of around  $\lambda_0/30$  at their resonance frequency. However, their performance has often been angle- and polarization-dependent, with a relatively narrow absorption bandwidth, due to the resonant behavior of metamaterial elements. Since modern practical applications require more sophisticated characteristics, such as larger bandwidths or multiple bands of operation as well as wide-angle and polarization-independent responses, a significant research has been triggered — and yet to be expected — for the improvement of these absorbers' overall behavior [10–19]. Apparently, this is a critical issue for various electromagnetic interference/electromagnetic compatibility (EMI/EMC) problems, like radar-cross section minimization from airplanes, steamboats and other vehicles, EMI protection owing to mobile phones and local area networks, light-trapping structures for photovoltaic systems or terahertz imaging devices [20–25].

In this paper, a class of ultra-thin, polarization-insensitive metamaterial structures that achieve high absorption in the microwave spectrum is introduced. To this aim, the new devices are implemented on inexpensive FR4 substrates, resulting in electrically-thin and hence, low-weight arrangements. Having determined the optimized unit-cell dimensions for an absorber operating in the middle of the microwave X-band (8.2–12.4 GHz), the outcomes of a thorough investigation regarding its competence in the case of oblique incidence are provided. Moreover, the absorption mechanism is qualitatively and quantitatively explained through further numerical simulations, which prove that the incident radiation is mainly dissipated inside the lossy dielectric volume. To the authors' best knowledge, such a quantitative analysis of the loss mechanism has not been previously conducted for metamaterial absorbers. In addition, measurements of a fabricated prototype are performed, showing a satisfactory agreement with the respective numerical results. Next, the scalability property of metamaterials is employed to create bandwidth-enhanced setups. For a dual-band structure, surface current distributions at the resonance frequencies are presented to interpret the underlying physics of the phenomenon. On the other hand, diverse possible unit-cell arrangements are explored for the triple-band case, leading to the selection of the optimal configuration. Finally, an idea for extending

the absorber’s bandwidth, deemed as the limiting case of a dual-band design with closely-placed absorption peaks, is briefly discussed.

## 2. ABSORBER DESIGN AND CHARACTERIZATION

For the design of an efficient and reliable metamaterial absorber, it is necessary to minimize both the reflection and transmission of the incident waves, exploiting the complex interactions of the metamaterial with the impinging radiation. Such a requirement stems from the definition of the absorption, obtained in terms of the  $S$ -parameters, as  $A(\omega) = 1 - T(\omega) - R(\omega)$ , where  $T(\omega) = |S_{21}|^2$  is the transmittance and  $R(\omega) = |S_{11}|^2$  the reflectance of the device, under development.

Consistent with the above conventions, the novel absorber is constructed via an electric ring resonator (ERR) [26], imprinted at the front face of a 1 mm thick FR4 dielectric substrate with a relative permittivity  $\epsilon_r = 4.1$  and a loss tangent  $\tan \delta = 0.025$ , as depicted in Figure 1. The specific ERR has been chosen because of its four-fold rotational symmetry around  $z$ -axis (i.e., it remains unchanged after every  $90^\circ$  rotation around  $z$ -axis), that renders the structure’s response insensitive to the polarization of the impinging waves. The opposite side of the dielectric spacer is covered by a full metallic plane

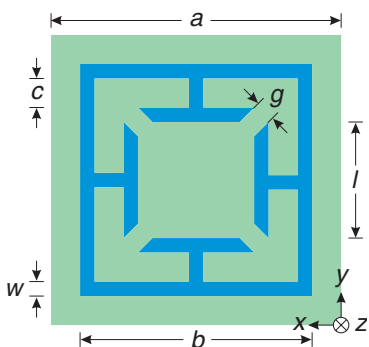


**Figure 1.** Optimized unit cell (front view) with  $a = 8$  mm,  $b = 4.2$  mm,  $c = 0.5$  mm,  $l = 1.9$  mm,  $g = 0.56$  mm, and  $w = 0.32$  mm. Thickness of the copper layer (blue color) is  $35 \mu\text{m}$ , while the thickness of the substrate (green color) is 1 mm.

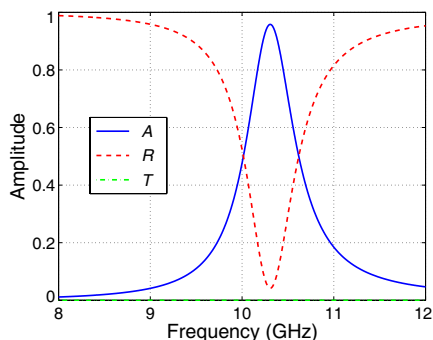


**Figure 2.** Absorption  $A(\omega)$ , reflectance  $R(\omega)$ , and transmittance  $T(\omega)$  of the proposed metamaterial absorber described in Figure 1. The peak value for the absorption is found to be 95.81% at 10.31 GHz.

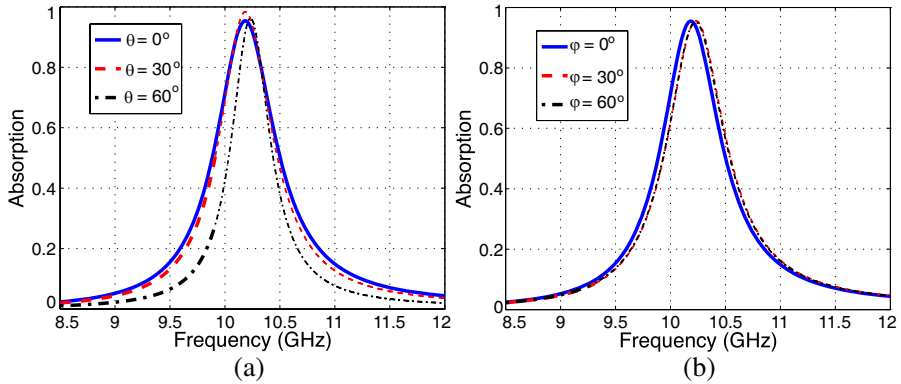


**Figure 3.** Absorption efficiency of the proposed device for obliquely-incident waves for two different cases. The wavevector lies on (a) the  $yz$ -plane ( $\theta$  variation) and (b) the  $xz$ -plane ( $\varphi$  variation).

so as to ensure zero transmission through the slab. Hence, only the reflectance is left to be minimized, which can be accomplished by matching the absorber's effective constitutive parameters to those of free space. For our simulations, the frequency domain solver of the CST MWS<sup>TM</sup> computational package [27] is utilized, where all metallic parts are modeled as copper with conductivity  $\sigma = 5.8 \cdot 10^7$  S/m and thickness  $t = 35 \mu\text{m}$ . Also, the pertinent periodic boundary conditions are applied along the  $x$  and  $y$  directions to account for an infinite array of unit cells, while a plane wave propagating along the  $z$ -axis serves as the incident radiation. To fulfill the matching criterion for the reflectance minimization, the dimensions of the unit cell are optimized by a genetic algorithm procedure. Specifically, the absorption, reflectance and transmittance of the optimized unit cell are shown in Figure 2. Observe that a single absorption peak of 95.81% occurs at 10.31 GHz, whereas the reflectance is minimized at the same frequency.

Since the ability of the proposed structure to absorb obliquely-incident waves is of equal importance to its performance in the case of normal incidence, an elaborate analysis of the absorption efficiency is conducted for two different scenarios. First, by retaining the electric field component parallel to the  $x$ -axis and modifying the angle (denoted as  $\theta$ ) between the wavevector and the  $z$ -axis on the  $yz$ -plane (see Figure 1 for axes definition), and second by keeping the magnetic field parallel to the  $y$ -axis and altering the angle (denoted as  $\varphi$ ) between the wavevector and the  $z$ -axis on the  $xz$ -plane. Note that, due to the absorber's four-fold rotational symmetry around the  $z$ -axis, these

two cases are equivalent to the propagation of TE- and TM-polarized plane waves, respectively. In this context, Figure 3(a) illustrates the simulation results for the variation of angle  $\theta$ , where a reduction of the absorption bandwidth is derived for very large incident angles, i.e.,  $\theta \geq 60^\circ$ . However, the maximum absorption is practically unaffected by the variation of the incidence angle in this case. Similar deductions can be drawn from Figure 3(b), concerning the variation of angle  $\varphi$ . As detected, very satisfactory absorption curves, centered almost at the same frequency as the one referring to normal incidence, are acquired even for especially large incidence angles. These promising results highlight the really wide-angle performance of the proposed setup; a key issue for several demanding applications mentioned in Section 1.

### 3. ABSORPTION MECHANISM INTERPRETATION

In this section, the absorption mechanism of the new structure is studied and explained both qualitatively and quantitatively. Generally, there are two absorption mechanisms, related to the conversion of electromagnetic energy into heat, namely: (a) losses due to the finite conductivity of the metallic parts (skin effect) and (b) losses due to the imaginary part of the substrate's dielectric permittivity.

First, in order to qualitatively assess the individual contribution of the prior mechanisms in the overall performance of our absorber, a set of simulations with different material combinations for the dielectric (lossless or lossy) and metallic parts (perfect electric conductor (PEC) or copper with finite conductivity) of the device are conducted. The corresponding absorption curves in the 8–12 GHz window are provided in Figure 4, which clearly illustrates the dominant role of dielectric

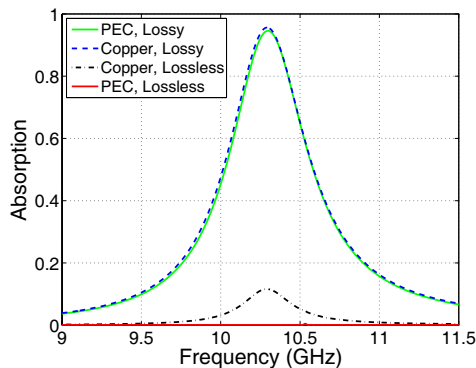


**Figure 4.** Absorption for various material combinations.

losses, since the curve remains practically unchanged after substituting the copper parts of the initial design with a PEC medium. However, in the case where copper is maintained for the metallic parts but the lossy FR4 substrate is substituted with a lossless one of the same dielectric constant, a maximum absorption of approximately 12% is observed, which can only be attributed to the presence of metallic losses.

This interesting result can be further supported by a quantitative analysis of the absorption phenomenon. Hence, an  $x$ -polarized incident plane wave propagating along the positive  $z$ -axis is considered, with

$$\mathbf{E} = E_0 \exp(-jk_0z) \hat{\mathbf{x}} = 2.425 \cdot 10^3 \exp(-jk_0z) \hat{\mathbf{x}}, \quad (1)$$

$$\mathbf{H} = \frac{E_0}{\eta_0} \exp(-jk_0z) \hat{\mathbf{y}} = 6.44 \exp(-jk_0z) \hat{\mathbf{y}}, \quad (2)$$

where  $k_0$  and  $\eta_0$  represent the free-space wavenumber and wave impedance, respectively. So, the Poynting vector is given by

$$\mathbf{S} = \frac{1}{2} \text{Re} \{ \mathbf{E} \times \mathbf{H}^* \} = \frac{1}{2} \frac{|E_0|^2}{\eta_0} \hat{\mathbf{z}} = 7.811 \cdot 10^3 \hat{\mathbf{z}}, \quad (3)$$

while, taking into account the size of the unit cell ( $8 \times 8 \text{ mm}^2$ ) at the transverse direction to the propagation, the total propagating (impinging) power is found to be  $P_p = 0.5 \text{ W}$ .

On the other hand, the power losses on the dielectric and metallic parts of the metamaterial absorber can be obtained through

$$P_d = \pi f \tan \delta \epsilon_0 \epsilon_r \iiint_{V_d} |E|^2 dV, \quad (4)$$

$$P_m = \frac{1}{2} \sqrt{\frac{\pi \mu f}{\sigma}} \iint_{S_m} |H|^2 dS, \quad (5)$$

with the two integrals evaluated over the substrate's volume,  $V_d$ , and the conductors' surface,  $S_m$ , correspondingly. Basically, these losses can be computed from the values of the numerically obtained electric and magnetic fields at the frequency of maximum absorption ( $A_{\text{max}} = 95.81\%$  for consistency at  $f = 10.35 \text{ GHz}$ ). Moreover, using the discretization of the previous simulations, we derive that  $P_d = 0.465 \text{ W}$  and  $P_m = 0.008 \text{ W}$ , adding up to  $P_l = P_d + P_m = 0.473 \text{ W}$ , which corresponds to 94.6% of the propagating power  $P_p$ . It should be stressed that this outcome is only about 1% different from the simulated peak value of 95.81%; a deviation attributed, mainly, to the discretization selected for the computation of the integrals in (4) and (5). This quantitative approach allows us to finally deduce that the dielectric losses are, indeed, at least two orders of magnitude higher than the metallic ones, thus constituting the main absorption mechanism of our absorber.

#### 4. EXPERIMENTAL REALIZATION AND MEASUREMENT SETUP

To verify the simulation results, a planar  $20 \times 20$  unit-cell prototype, illustrated in Figure 5(a), has been fabricated through standard photolithographic techniques on an FR4 substrate, according to the features specified in Section 2. For the measurement of its reflectance, a quasi-monostatic configuration with fixed receiving and transmitting 10 dB-gain WR90 horn antennas, operating at the microwave X-band (8.2–12.4 GHz), has been realized. The separation angle between the two antennas, connected to the network analyzer via low-loss coaxial cables as in Figure 5(b), has been set to  $\varphi_s = 3^\circ$ . Initially, the noise floor threshold has been obtained by measuring the transmission between the antennas in the absence of any sample, in order to be afterwards eliminated by suitably calibrating the network analyzer.

Subsequently, the metamaterial sample has been placed in the middle of an array of conventional pyramidal absorbing media to cancel any scattering from the environment. The distance between the sample and the antennas has been chosen as  $h = 20$  cm, so that the far field condition  $2D^2/\lambda \simeq 13$  cm (with  $D = 4$  cm the largest dimension of the antenna and  $\lambda \simeq 2.5$  cm the wavelength at the higher frequency of the X-band) is amply satisfied. The overall measurement arrangement is normalized with respect to a reference one, where the sample is replaced with a copper sheet of identical size. Experimental results, displayed in Figure 6 together with the simulated absorption curve, certify the advantages of the proposed wide-angle design, yet also reveal that the absorption band is wider than the simulated one. This reasonable and anticipated difference can be primarily attributed to fabrication tolerances and fluctuation of the substrate's electric characteristics around their nominal values.



**Figure 5.** (a) Fabricated metamaterial absorber prototype with  $20 \times 20$  unit cells. (b) Its laboratory experimental setup.

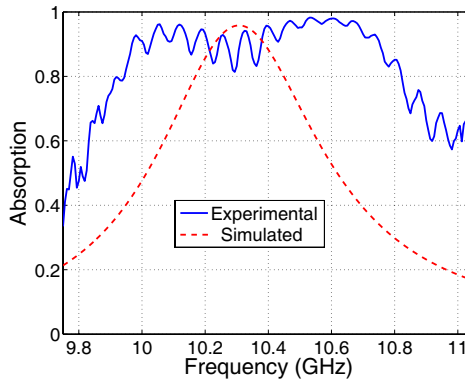


**Figure 6.** Measured absorption for the proposed structure depicted in Figure 5(a).

## 5. DESIGN OF BANDWIDTH-ENHANCED ABSORBERS

Based on the previous analysis, a family of competent multi-band and broadband metamaterial absorbers are synthesized via the proper scaling of the original device. In fact, our designs exploit the scalability property of metamaterials, which offers several flexible degrees of freedom. Explicitly, by multiplying the dimensions of the original ERR along the  $x$ - and  $y$ -axis by a scaling factor  $s$ , the center absorption frequency can be downshifted ( $s > 1$ ) or upshifted ( $s < 1$ ), whereas the absorption curve retains its initial shape and fractional bandwidth. Note that, no scaling is applied along the  $z$ -direction, since the metal thickness has no effect on the overall behavior of the absorbers.

### 5.1. Dual-band Absorber

For a dual-band metamaterial absorber, four ERRs are imprinted at the front face of an FR4 substrate, as in Figure 7. In this configuration, the ERRs placed along the same diagonal share the same dimensions. Two of them have the dimensions of the original structure ( $s_1 = 1.0$ ), while the other two are scaled by  $s_2 = 0.9$ . The opposite side of the dielectric is covered by a full copper plane to guarantee zero transmission through the slab, as explained in Section 2. In this context, the simulated absorption curve of the resulting device is given in Figure 8, where two distinct absorption peaks can be detected. The first peak is located at the frequency of 10.45 GHz with a maximum of 99.31%, while the second one of 96.13% occurs at 11.65 GHz.

Furthermore, Figure 9 presents the respective surface current

distributions at the two resonant frequencies in order to better interpret the absorption mechanism of the dual-band structure. Specifically, at 10.45 GHz, surface currents indicate the resonant behavior of the larger ERRs, whereas at 11.65 GHz the electric resonance of the smaller ERRs becomes apparent. These outcomes suggest that the combination of unit cells designed for different absorption frequencies can yield the superposition of their absorptive spectra, thus providing a significant verification of our notion for the realization of multi-band components. Notice, nevertheless, that the first resonant frequency of the device has

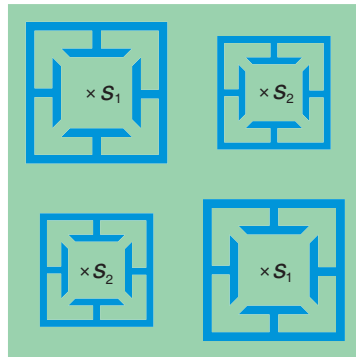


**Figure 7.** Unit cell of a dual-band metamaterial absorber, consisting of four appropriately scaled ERRs. The corresponding scaling factors are selected as  $s_1 = 1.0$  and  $s_2 = 0.9$ .

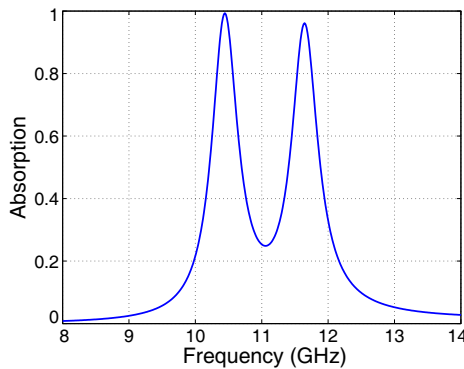


**Figure 8.** Absorption spectrum of the dual-band structure. The first peak reaches a maximum of 99.31% at 10.45 GHz, while the second one corresponds to a maximum value of 96.13% at 11.65 GHz.

been slightly shifted from 10.31 GHz (originally designed in Section 2) to 10.45 GHz, as a result of the coupling between the different ERRs in the array. This coupling degrades by increasing the unit-cell size, at the cost of a small reduction in the absorption peaks (not shown here).

## 5.2. Triple-band Absorbers

The design concept of the dual-band structure can be easily extended to the implementation of more complicated multi-band devices. Such a setup is the triple-band absorber of Figure 10. The novel unit cell

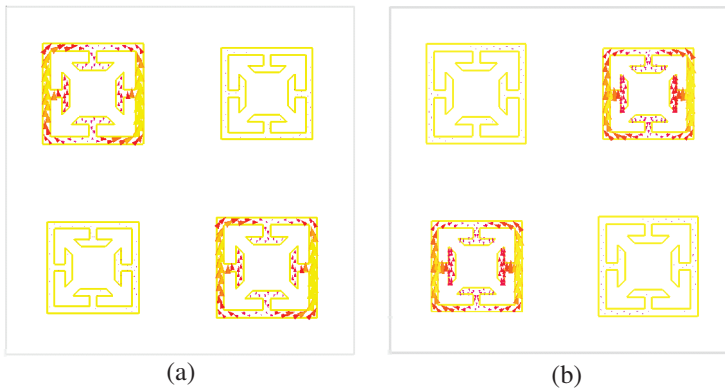


**Figure 9.** Surface current distributions on the front side of the dual-band absorber at (a) 10.45 GHz and (b) 11.65 GHz.

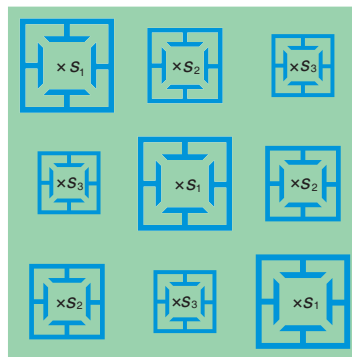


**Figure 10.** Unit cell of a triple-band absorber consisting of nine properly scaled ERRs. The values of the scaling factors are  $s_1 = 1.0$ ,  $s_2 = 0.8$ , and  $s_3 = 0.7$ .

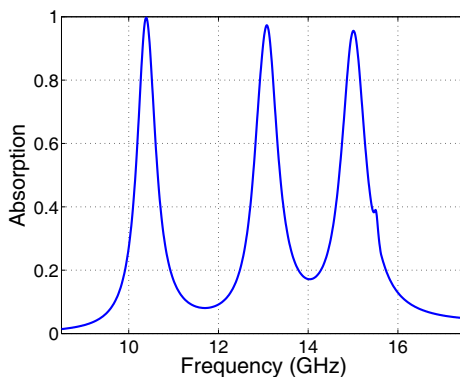


**Figure 11.** Absorption spectrum of the triple-band structure. The first peak reaches a maximum of 99.73% at 10.39 GHz, the second peak corresponds to the value of 97.32% at 13.08 GHz, and the third one to the value of 95.56% at 15.01 GHz.

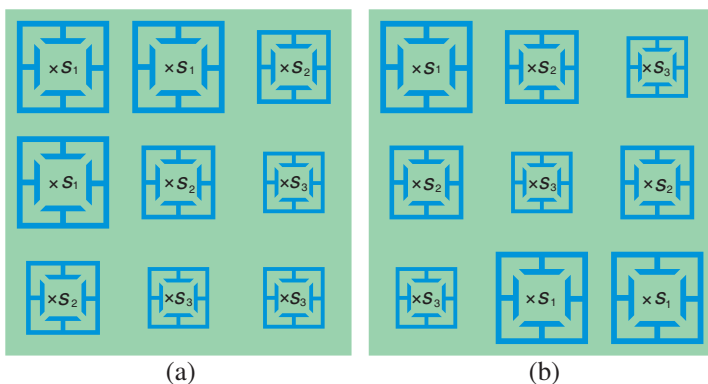


**Figure 12.** Two variants of the triple-band absorber of Figure 10. (a) Variant 1. (b) Variant 2.

extends to a set of nine ERR elements, with the selected scaling factors being  $s_1 = 1.0$ ,  $s_2 = 0.8$ , and  $s_3 = 0.7$  for the larger, medium, and smaller ERRs, respectively. Simulation results are shown in Figure 11, where three distinct absorption peaks can be promptly observed. In particular, the first peak approaches a maximum of 99.73% at 10.39 GHz, the second one reaches a maximum 97.32% value at 13.08 GHz, while the third one a 95.56% value at 15.01 GHz. The shift of the first resonance frequency (from 10.31 GHz to 10.39 GHz) is lower compared to the dual-band case, since adjacent ERRs are now

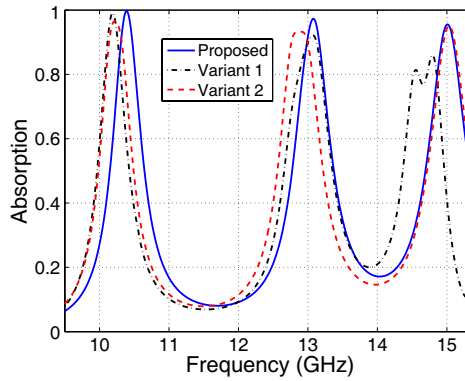


**Figure 13.** Comparison of the proposed triple-band absorber and the two variants of Figure 12.

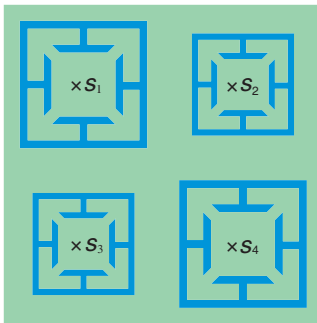


**Figure 14.** Unit cell of a broadband metamaterial absorber, consisting of four properly scaled ERRs. The values of the scaling factors are  $s_1 = 0.98$ ,  $s_2 = 0.99$ ,  $s_3 = 1.00$ , and  $s_4 = 1.01$ .

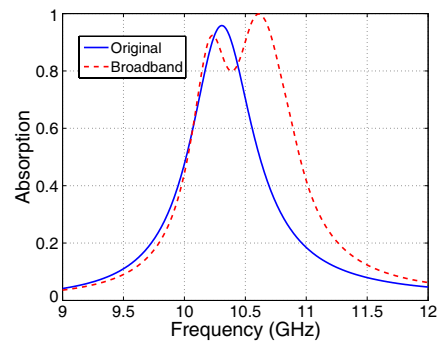


**Figure 15.** Comparison of the original absorber to its broadband counterpart.

scaled with smaller factors than in the previous application.

Moreover, in order to investigate the effect of the ERRs relative arrangement on the device's overall performance, the same resonators can be combined in several ways inside the unit cell. To this goal, two indicative variants of the triple-band absorber of Figure 10 are taken into account, as shown in Figure 12. The outcomes of the comparison are displayed in Figure 13, unveiling that the structure of Figure 10 is, indeed, the optimal choice for the specific triple-band absorber.

### 5.3. Development of Broadband Absorbers

In general, metamaterial absorbers exhibit a limited operational bandwidth, due to the resonant behavior of their constituent elements, which usually varies around the value of 5% in terms of the full width at half maximum (FWHM) gauge. Actually, the realization of broadband metamaterial absorbers [28–30] can be seen as the borderline case of multi-band designs, with scaling factors of the respective ERRs approaching unity. To substantiate the essence of this idea, four ERRs are imprinted at the front face of an FR4 substrate, with its opposite side covered by a full copper plane, as depicted in Figure 14. Each ERR is scaled by a factor  $s_i$ , where  $i = 1, 2, 3, 4$ . For  $s_1 = 0.98$ ,  $s_2 = 0.99$ ,  $s_3 = 1.00$ , and  $s_4 = 1.01$ , Figure 15 indicates a wider frequency band of high absorption, as compared to that of Figure 1. Particularly, FWHM has increased from 5.82% in the initial design to the value of 8.78%, whereas, although two distinct peaks can be clearly identified in the resulting curve, the broadband structure absorbs over 80% for twice the frequency band than the original structure.

## 6. CONCLUSIONS

A new class of polarization-independent, multi-band, and broadband metamaterial absorber designs for contemporary EMC applications has been proposed in this paper. According to the simulated results, the developed unit cell, which comprises a symmetrical ERR structure imprinted on a lossy, metal-backed FR4 substrate, provides an absorption of around 96% at the target frequency for both polarizations and over a wide range of incident angles. The fabrication and measurement of a prototype for the validation of the numerically predicted performance characteristics has also been presented, while a thorough quantitative interpretation of the power loss mechanism within the device has been performed. This analysis proved that, indeed, dielectric losses dominate the behavior of such components in the microwave spectrum, where metals can be practically considered as perfect electric conductors. Also, by employing the scalability property of the metamaterial elements, we achieved several multiple absorption peaks via the combination of properly scaled ERRs in a new planar composite unit cell, thus extending the initially proposed structure to dual- and triple-band setups. Finally, the possibility to increase the FWHM of the original absorber by a factor of about 50% has been exemplified as the borderline case of a passive (i.e., without use of active elements) dual-band arrangement with closely-located resonances.

## ACKNOWLEDGMENT

This research has been co-financed by the EU (European Social Fund — ESF) and Greek national funds through the Operational Program “Education and Lifelong Learning” of the National Strategic Reference Framework (NSRF) — Research Funding Program: Heracleitus II. Investing in knowledge society through the European Social Fund.

## REFERENCES

1. Caloz, C. and T. Itoh, *Electromagnetic Metamaterials: Transmission Line Theory and Microwave Applications*, John Wiley & Sons, New York, 2006.
2. Marqués, R., F. Martín, and M. Sorolla, *Metamaterials with Negative Parameters: Theory, Design, and Microwave Applications*, John Wiley & Sons, New York, 2008.
3. Smith, D. R., D. C. Vier, T. Koschny, and C. M. Soukoulis, “Electromagnetic parameter retrieval from inhomogeneous metamaterials,” *Phys. Rev. E*, Vol. 71, 036617, 1–11, 2005.
4. Landy, N. Y., S. Sajuyigbe, J. J. Mock, D. R. Smith, and W. J. Padilla, “Perfect metamaterial absorber,” *Phys. Rev. Lett.*, Vol. 100, 207402, 1–4, 2008.
5. Li, M.-H., H.-L. Yang, and X.-W. Hou, “Perfect metamaterial absorber with dual bands,” *Progress In Electromagnetics Research*, Vol. 108, 37–49, 2010.
6. Bilotti, F., A. Toscano, K. B. Alici, E. Ozbay, and L. Vegni, “Design of miniaturized narrowband absorbers based on resonant-magnetic inclusions,” *IEEE Trans. Electromagn. Compat.*, Vol. 53, No. 63, 63–72, 2011.
7. Liu, H. X., B. F. Yao, L. Li, and X. W. Shi, “Analysis and design of thin planar absorbing structures using Jerusalem cross slot,” *Progress In Electromagnetic Research B*, Vol. 31, 261–281, 2011.
8. Zhu, W., X. Zhao, B. Gong, L. Liu, and B. Su, “Optical metamaterial absorber based on leaf-shaped cells,” *Appl. Phys. A — Mater.*, Vol. 102, No. 1, 147–151, 2011.
9. Ye, D., Z. Wang, Z. Wang, K. Xu, B. Zhang, J. Huangfu, C. Li, and L. Ran, “Towards experimental perfectly-matched layers with ultra-thin metamaterial surfaces,” *IEEE Trans. Antennas Propag.*, Vol. 60, No. 11, 5164–5172, 2012.
10. Zhu, B., Z. Wang, C. Huang, Y. Feng, J. Zhao, and T. Jiang, “Polarization insensitive metamaterial absorber with

- wide incident angle,” *Progress In Electromagnetics Research*, Vol. 101, 231–239, 2010.
11. Lee, J. and S. Lim, “Bandwidth-enhanced and polarization-insensitive metamaterial absorber using double resonance,” *Electron. Lett.*, Vol. 47, 8–9, 2011.
  12. He, X. J., Y. Wang, J. M. Wang, and T. L. Gui, “Dual-band terahertz metamaterial absorber with polarization insensitivity and wide incident angle,” *Progress In Electromagnetic Research*, Vol. 115, 381–397, 2011.
  13. Li, H., L. H. Yuan, B. Zhou, X. P. Shen, Q. Cheng, and T. J. Cui, “Ultrathin multiband gigahertz metamaterial absorbers,” *J. Appl. Phys.*, Vol. 110, 014909, 1–8, 2011.
  14. Zhao, Y., F. Chen, H. Chen, N. Li, Q. Shen, and L. Zhang, “The microstructure design optimization of negative index metamaterials using genetic algorithm,” *Progress In Electromagnetics Research Letters*, Vol. 22, 95–108, 2011.
  15. Shen, X., T. J. Cui, J. Zhao, H. F. Ma, W. X. Jiang, and H. Li, “Polarization-independent wide-angle triple-band metamaterial absorber,” *Opt. Express*, Vol. 19, 9401–9407, 2011.
  16. Fallahzadeh, S., K. Forooraghi, and Z. Atlasbaf, “Design, simulation and measurement of a dual linear polarization insensitive planar resonant metamaterial absorber,” *Progress In Electromagnetic Research Letters*, Vol. 35, 135–144, 2012.
  17. Lu, L., S. Qu, H. Ma, F. Yu, S. Xia, Z. Xu, and P. Bai, “A polarization-independent wide-angle dual directional absorption metamaterial absorber,” *Progress In Electromagnetic Research M*, Vol. 77, 191–201, 2012.
  18. Ye, Q., Y. Liu, H. Lin, M. Li, and H. Yang, “Multi-band metamaterial absorber made of multi-gap SRRs structure,” *Appl. Phys. A — Mater.*, Vol. 107, No. 1, 155–160, 2012.
  19. Lee, H.-M and H.-S. Lee, “A metamaterial based microwave absorber composed of coplanar electric-field-coupled resonator and wire array,” *Progress In Electromagnetic Research C*, Vol. 34, 111–121, 2013.
  20. Oraizi, H., A. Abdolali, and N. Vaseghi, “Application of double zero metamaterials as radar absorbing materials for the reduction of radar cross section,” *Progress In Electromagnetic Research*, Vol. 101, 323–337, 2010.
  21. Tao, H., C. M. Bingham, D. Pilon, K. Fan, A. C. Strkwerda, D. Shrekenhammer, W. J. Padilla, X. Zhang, and R. D. Averitt, “A dual band terahertz metamaterial absorber,” *J. Appl. Phys.*,

- Vol. 43, 22510, 1–5, 2010.
22. Veysi, M., M. Kamyab, J. Moghaddasi, and A. Jafargholi, “Transmission phase characterizations of metamaterial covers for antenna application,” *Progress In Electromagnetics Research Letters*, Vol. 21, 49–57, 2011.
  23. Jiang, Z. H., S. Yun, F. Toor, D. H. Werner, and T. S. Mayer, “Conformal dual-band near-perfectly absorbing mid-infrared metamaterial coating,” *ACS Nano*, Vol. 5, No. 6, 4641–4647, 2011.
  24. Kuznetsov, S. A., A. G. Paulish, A. V. Gelfand, P. A. Lazorskiy, and V. N. Fedorinin, “Matrix structure of metamaterial absorbers for multispectral terahertz imaging,” *Progress In Electromagnetic Research*, Vol. 122, 93–103, 2012.
  25. Koledintseva, M. Y., J. Huang, J. L. Drewniak, R. E. DuBroff, and B. Archambeault, “Modeling of metasheets embedded in dielectric layers,” *Progress In Electromagnetics Research B*, Vol. 44, 89–116, 2012.
  26. Chen, H. T., J. F. O’Hara, A. J. Taylor, R. D. Averitt, C. Highstrete, M. Lee, and W. J. Padilla, “Complementary planar terahertz metamaterials,” *Opt. Express*, Vol. 15, 1084–1095, 2007.
  27. Computer Simulation Technology, *CST MWS<sup>TM</sup>: Computer Simulation Technology: Microwave Studio*, 2010.
  28. Gu, S., J. P. Barrett, T. H. Hand, B. I. Popa, and S. A. Cummer, “A broadband low-reflection metamaterial absorber,” *J. Appl. Phys.*, Vol. 108, 064913, 1–6, 2010.
  29. Sun, J., L. Liu, G. Dong, and J. Zhou, “An extremely broad band metamaterial absorber based on destructive interference,” *Opt. Express*, Vol. 19, No. 22, 21155–21162, 2011.
  30. Cheng, Y. Z., Y. Wang, Y. Nie, R. Z. Gong, X. Xiong, and X. Wang, “Design, fabrication and measurement of a broadband polarization-insensitive metamaterial absorber based on lumped elements,” *J. Appl. Phys.*, Vol. 111, 044902, 1–4, 2012.